SIAM J. SCI. COMPUT.
Vol. 38, No. 2, pp. A668–A690

CONSTRAINT PRECONDITIONING FOR THE COUPLED STOKES–DARCY SYSTEM*

PRINCE CHIDYAGWAI†, SCOTT LADENHEIM‡, AND DANIEL B. SZYLD§

Abstract. The use of a constraint (indefinite) preconditioner for the iterative solution of the linear system arising from the finite element discretization of coupled Stokes–Darcy flow is studied. Spectral and field-of-values bounds for the preconditioned system which are independent of the underlying mesh size are presented. Numerical experiments on several two- and three-dimensional problems illustrate the effectiveness of our approach.

Key words. Stokes–Darcy flow, iterative methods, indefinite preconditioners, constraint preconditioners, spectral equivalence, field-of-values equivalence

AMS subject classifications. 65F08, 65N30, 76S05

DOI. 10.1137/15M1032156

1. Introduction.

The coupled Stokes–Darcy model is an important set of partial differential equations which describes the interaction between free flow and porous media flow. In one subregion of the domain, a freely flowing fluid moves according to the Stokes equations, and in the other region, the flow is governed by Darcy's law. The equations are coupled together by conditions across the interface of the two subregions. Physically, the model can represent a freely flowing fluid over a porous medium, or other phenomena such as certain filtration processes. For further examples of the various application areas of the coupled Stokes–Darcy model, see, e.g., [12] and the references therein.

A customary approach for the numerical solution of the coupled Stokes–Darcy problem is by the finite element method; see, e.g., [10, 11, 12, 17, 28]. Here, we consider solving the fully coupled system in an all-at-once approach, as was considered, for instance, in [10, 11]. This is in contrast to other approaches that decouple the two systems. In the decoupled approach, the Stokes and Darcy equations are solved as separate subproblems with appropriate conditions for updating and exchanging information across the interface of the two subregions; see, e.g., [23, 25]. One main benefit of decoupling the system is that rather than solving one large system, two smaller subproblems are solved for which well-known, fast solution methods exist. However, the reason we use the all-at-once approach is that it more accurately models the underlying physics of the problem. As we shall see, one can take advantage of the fast solvers for the subproblems with the appropriate preconditioning implementation.

*Submitted to the journal's Methods and Algorithms for Scientific Computing section July 23, 2015; accepted for publication (in revised form) December 4, 2015; published electronically March 1, 2016. This research was supported in part by the National Science Foundation through major research instrumentation grant CNS-09-5884.

http://www.siam.org/journals/sisc/38-2/M103215.html

†Department of Mathematics and Statistics, Loyola University Maryland, Baltimore, MD 21210 (pchidyagwai@loyola.edu). This author's work was supported in part by the U.S. National Science Foundation under grant DMS-1115269.

‡Current address. IT-Building, School of Computer Science, University of Manchester, Manchester M13 9PL, UK (scott.ladenheim@manchester.ac.uk).

§Department of Mathematics, Temple University, Philadelphia, PA 19122 (szyld@temple.edu). This author's work was supported in part by the U.S. National Science Foundation under grants DMS-1115520 and DMS-1418882.

At the core of obtaining the finite element solution for the fully coupled Stokes–Darcy system, a large, sparse linear system of saddle point form must be solved. Saddle point matrices are an important class of matrices that arise in a wide variety of computational science and engineering applications; see [5] for a detailed list. The fact that these saddle point matrices are large and sparse makes them amenable to solution by Krylov subspace iterative methods; see, e.g., [33]. A fundamental property of saddle point matrices is that they are indefinite, having both positive and negative eigenvalues. A preconditioner for the Krylov subspace method of choice is essential for convergence in a reasonable number of iterations and time.

Here, we want to study the solution of the fully coupled, nonsymmetric system using preconditioned GMRES with a constraint (or indefinite) preconditioner. Standard block diagonal and block lower triangular preconditioners have been considered for the Stokes–Darcy system in [10]. There, the authors used the norm-equivalence theory of [24] and proved that the spectra of the preconditioned operators with these two types of preconditioners were bounded independently of the mesh width. Furthermore, the numerical experiments in [10] demonstrate mesh-independent convergence of the GMRES algorithm for these preconditioners in two-dimensional (2-D) problems.

The constraint (indefinite) preconditioner we are proposing mimics the structure of the original saddle point system and has been analyzed, for example, in [21, 27, 32]. This type of preconditioner is often referred to as a constraint preconditioner because the constraints of the problem are retained by the preconditioner. In this paper, we extend the results of [24] to constraint preconditioners, namely, we prove that constraint preconditioners are norm- and field-of-values-equivalent to the coupled Stokes–Darcy system. By the field-of-values- (f.o.v.-) equivalence theory of [24], the number of GMRES iterations to converge for the constraint preconditioned Stokes–Darcy operator is bounded independently of the mesh width.

The application of this constraint preconditioner entails the solution of (smaller) linear systems. These smaller subsystems can be solved exactly using a direct method like an LU decomposition. Exact methods are effective for 2-D coupled flow problems where the bandwidth of the block matrices is not that large. We remark that the f.o.v.-analysis for constraint preconditioners holds only for exact block solves. However, for large systems, especially those from three-dimensional (3-D) calculations, one needs to solve these intermediate systems inexactly, i.e., up to an inner tolerance using an iterative method. We show that by using multigrid methods [9, 19], our spectral analysis is maintained and though f.o.v.-equivalence in this case is lost, the overall method with an inexact version of the preconditioner is still effective.

The paper is structured as follows. In section 2, we review the governing equations of the coupled Stokes–Darcy model along with the corresponding weak form. We then review the derivation of the linear system of interest to be solved. In section 3, we introduce the preconditioners to be considered. In addition, we prove that the use of a constraint preconditioner leads to residual convergence rates that are independent of the mesh width in an appropriately defined norm, as was done in [10, 24]. In section 4, we discuss the inexact implementation of the preconditioners. In section 5, we present numerical experiments illustrating our theoretical analysis and showing that constraint preconditioning can indeed be an effective tool. Concluding remarks are given in section 6.

2. The coupled Stokes–Darcy model. We consider the coupled flow problem on a computational domain Ω partitioned into two nonoverlapping domains Ω_1 and Ω_2 separated by a polygonal interface Γ_{12}; see Figure 1. The flow in Ω_1 is described

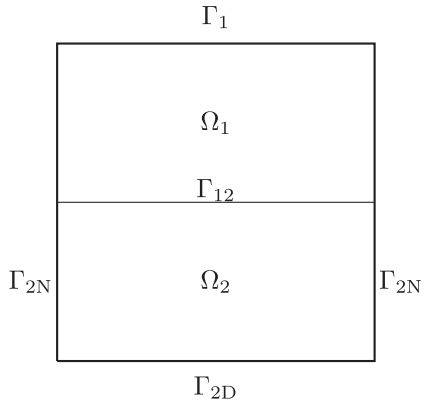

FIG. 1. *The 2-D coupled Stokes–Darcy computational domain.*

by the Stokes equations

$$-\nabla \cdot (2\nu D(\mathbf{u}_1) - p_1 \mathbf{I}) = \mathbf{f}_1 \quad \text{in } \Omega_1, \tag{2.1a}$$

$$\nabla \cdot \mathbf{u}_1 = 0 \quad \text{in } \Omega_1, \tag{2.1b}$$

$$\mathbf{u}_1 = 0 \quad \text{on } \Gamma_1 = \partial\Omega_1 \cap \partial\Omega. \tag{2.1c}$$

The velocity and pressure in Ω_1 are denoted by $\mathbf{u}_1$, p_1, respectively. The coefficient $\nu > 0$ is the kinematic viscosity, the function $\mathbf{f}_1$ is an external force acting on the fluid, $\mathbf{I}$ is the identity matrix, and $D(\mathbf{u}_1) = \frac{1}{2}(\nabla \mathbf{u}_1 + \nabla \mathbf{u}_1^T)$ is the rate of strain tensor.

The boundary of the porous medium $\Gamma_2 = \partial\Omega \cap \partial\Omega_2$ is partitioned into disjoint parts Γ_{2N} and Γ_{2D}, the Dirichlet and Neumann boundaries, respectively, with the condition $|\Gamma_{2D}| > 0$, i.e., that the Dirichlet portion of the boundary has positive measure. The flow in Ω_2 is modeled by Darcy's law

$$-\nabla \cdot \mathbf{K} \nabla p_2 = f_2 \quad \text{in } \Omega_2, \tag{2.2a}$$

$$p_2 = g_D \quad \text{on } \Gamma_{2D}, \tag{2.2b}$$

$$\mathbf{K} \nabla p_2 \cdot \mathbf{n}_2 = g_N \quad \text{on } \Gamma_{2N}. \tag{2.2c}$$

The Darcy pressure in Ω_2 is denoted by p_2. The Darcy velocity $\mathbf{u_2}$ is obtained by numerically differentiating the Darcy pressure

$$\mathbf{u}_2 = -\mathbf{K} \nabla p_2 \quad \text{in } \Omega_2. \tag{2.3}$$

The symmetric positive definite (s.p.d.) matrix $\mathbf{K}$ represents the hydraulic conductivity of the fluid in the porous medium, and the vector $\mathbf{n}_2$ denotes the outward unit normal vector to Γ_{2N}. We consider isotropic flow in the porous medium so that $\mathbf{K} = \kappa \mathbf{I}$ for some constant κ. The model is completed by specifying the following coupling (interface) conditions on Γ_{12}. Let $\mathbf{n}_{12}$ and $\boldsymbol{\tau}_{12}$ denote the unit normal vector directed from Ω_1 towards Ω_2 and unit tangential vector to the interface, respectively. The interface conditions are

$$\mathbf{u}_1 \cdot \mathbf{n}_{12} = -\mathbf{K} \nabla p_2 \cdot \mathbf{n}_{12}, \tag{2.4a}$$

$$(-2\nu D(\mathbf{u}_1)\mathbf{n}_{12} + p_1 \mathbf{n}_{12}) \cdot \mathbf{n}_{12} = p_2, \tag{2.4b}$$

$$\mathbf{u}_1 \cdot \boldsymbol{\tau}_{12} = -2\nu G(D(\mathbf{u}_1)\mathbf{n}_{12}) \cdot \boldsymbol{\tau}_{12}, \tag{2.4c}$$

where (2.4a) ensures mass conservation across the interface, (2.4b) ensures the balance of normal forces across the interface, and (2.4c) is the Beavers–Joseph–Saffman (BJS) law, where G is an experimentally determined constant [4, 31]. In the numerical experiments that follow we set $G = 1.0$ for 2-D test problems with known smooth solutions. In the case of more practical test problems in 3-D we follow the approach outlined in [4] by defining $G = \frac{\alpha}{\sqrt{\kappa}}$ where the parameter α depends on the nature of the porous medium. In the case of our 3-D examples we set $\alpha = 0.1$, which corresponds to one of the porous media tested in numerical experiments justifying the BJS condition in [4].

We consider the standard finite element formulation of the coupled Stokes–Darcy system. We first introduce the weak form of (2.1), (2.2), and (2.4). Let

$$\boldsymbol{X}_1 = \{\mathbf{v}_1 \in (H^1(\Omega_1))^2 : \ \mathbf{v}_1 = 0 \text{ on } \Gamma_1\}, \quad Q_1 = L^2(\Omega_1),$$

be the Stokes velocity and pressure spaces, respectively, and let

$$Q_2 = \{q_2 \in H^1(\Omega_2) : \ q_2 = 0 \text{ on } \Gamma_{2\mathrm{D}}\}$$

be the Darcy pressure space. Then the weak formulation becomes the following: find $\mathbf{u}_1 \in \boldsymbol{X}_1$, $p_1 \in Q_1$, and $p_2 \in Q_2$ such that

$$a(\mathbf{u}_1, p_2; \mathbf{v}_1, q_2) + b(\mathbf{v}_1, p_1) = \mathbf{f}(\mathbf{v}_1, q_2) \quad \forall \mathbf{v}_1 \in \boldsymbol{X}_1, \ \forall q_2 \in Q_2, \tag{2.5a}$$

$$b(\mathbf{u}_1, q_1) = 0 \quad \forall q_1 \in Q_1, \tag{2.5b}$$

where

$$a(\mathbf{u}_1, p_2; \mathbf{v}_1, q_2) = a_{\Omega_1}(\mathbf{u}_1, \mathbf{v}_1) + a_{\Omega_2}(p_2, q_2) + a_{\Gamma_{12}}(\mathbf{u}_1, p_2; \mathbf{v}_1, q_2),$$

$$b(\mathbf{u}_1, q_1) = -\int_{\Omega_1} (\nabla \cdot \mathbf{u}_1) q_1 \, dx,$$

and

$$a_{\Omega_1}(\mathbf{u}_1, \mathbf{v}_1) = 2\nu \int_{\Omega_1} D(\mathbf{u}_1) : D(\mathbf{v}_1) + \frac{1}{G} \int_{\Gamma_{12}} (\mathbf{u}_1 \cdot \boldsymbol{\tau}_{12})(\mathbf{v}_1 \cdot \boldsymbol{\tau}_{12}),$$

$$a_{\Omega_2}(p_2, q_2) = \int_{\Omega_2} \mathbf{K} \nabla p_2 \cdot \nabla q_2,$$

$$a_{\Gamma_{12}}(\mathbf{u}_1, p_2; \mathbf{v}_1, q_2) = \int_{\Gamma_{12}} (p_2 \mathbf{v}_1 - q_2 \mathbf{u}_1) \cdot \mathbf{n}_{12}.$$

The right-hand side is

$$\mathbf{f}(\mathbf{v}_1, q_2) = \int_{\Omega_1} \mathbf{f}_1 \cdot \mathbf{v}_1 + \int_{\Omega_2} f_2 q_2 + \int_{\Gamma_{2\mathrm{N}}} g_{\mathrm{N}} q_2. \tag{2.7}$$

In addition, we introduce the norms

$$\|(p_2, \mathbf{u}_1)\|_{Q_2 \times X_1} = \left(\|\mathbf{K}^{1/2} p_2\|^2_{H^1(\Omega_2)} + \|D(\mathbf{u}_1)\|^2_{L^2(\Omega_1)} \right)^{1/2}, \tag{2.8a}$$

$$\|p_1\|_{Q_1} = \|p_1\|_{L^2(\Omega_1)}, \tag{2.8b}$$

which are used in the analysis in section 3. We refer the reader to [11] and references therein for further details on the weak formulation of the coupled problem. The finite

element discretization of (2.5) proceeds by choosing conforming finite element spaces $\boldsymbol{X}_1^h \subset \boldsymbol{X}_1$ and $Q_1^h \subset Q_1$ satisfying the discrete inf-sup condition to approximate the Stokes velocity and pressure, respectively. Examples include the MINI finite element spaces [2] or the Taylor–Hood elements [13, 34]. The Darcy pressure is approximated by the finite element space $Q_2^h \subset Q_2$. The Darcy pressure space Q_2^h is chosen to be piecewise continuous polynomials. We consider piecewise linear polynomials for 2-D problems and piecewise quadratics for 3-D. We note that regardless of the choice of finite element spaces $(\boldsymbol{X}_1^h, Q_1^h, Q_2^h)$ the discrete version of (2.5) is the system of equations

$$\mathcal{A}\mathbf{x} = \begin{bmatrix} A_{\Omega_2} & A_{\Gamma_{12}}^T & 0 \\ -A_{\Gamma_{12}} & A_{\Omega_1} & B^T \\ 0 & B & 0 \end{bmatrix} \begin{bmatrix} p_2 \\ \mathbf{u}_1 \\ p_1 \end{bmatrix} = \begin{bmatrix} f_{2,h} \\ \mathbf{f}_{1,h} \\ g_h \end{bmatrix} = \mathbf{b}, \tag{2.9}$$

where the blocks $A_{\Omega_1}, A_{\Omega_2}$ correspond to the discretized versions of the bilinear forms $a_{\Omega_1}(\cdot,\cdot)$ and $a_{\Omega_2}(\cdot,\cdot)$, respectively, B corresponds to the discretized version of the mixed bilinear form $b(\cdot,\cdot)$, and $A_{\Gamma_{12}}$ and its transpose correspond to a discretized version of the bilinear form $a_{\Gamma_{12}}(\cdot,\cdot)$. In addition, as the mesh width is decreased, the dimension of the matrix $\mathcal{A}$ increases.

Setting

$$A = \begin{bmatrix} A_{\Omega_2} & A_{\Gamma_{12}}^T \\ -A_{\Gamma_{12}} & A_{\Omega_1} \end{bmatrix}, \quad C = \begin{bmatrix} 0 & B \end{bmatrix},$$

it is easy to see that the system of equations (2.9) is of saddle point form (see, e.g., [5])

$$\mathcal{A} = \begin{bmatrix} A & C^T \\ C & 0 \end{bmatrix}. \tag{2.10}$$

In the discrete case, when $p_2, \mathbf{u}_1$, and p_1 are the vectors of coefficients for the finite element basis functions, we have the corresponding discrete norms

$$\|(p_2, \mathbf{u}_1)\|_{Q_2^h \times X_1^h} = \left(\langle p_2, p_2\rangle_{A_{\Omega_2}} + \langle \mathbf{u}_1, \mathbf{u}_1\rangle_{A_{\Omega_1}}\right)^{1/2}, \tag{2.11a}$$

$$\|p_1\|_{Q_1^h} = \langle p_1, q_1\rangle_{M_p}^{1/2}, \tag{2.11b}$$

where $\langle \mathbf{v}, \mathbf{v}\rangle_H = \langle H\mathbf{v}, \mathbf{v}\rangle = \mathbf{v}^T H\mathbf{v}$ for an s.p.d. matrix H, and M_p denotes the mass matrix for the Stokes pressure space. Note that when $H = I$ we recover the standard Euclidian inner product whose induced matrix norm is denoted by $\|\cdot\|_2$. This vector norm induces the following matrix norm for matrices $M \in \mathbb{R}^{m\times n}$:

$$\|M\|_H = \max_{\mathbf{v}\in\mathbb{R}^n\setminus\{0\}} \frac{\|M\mathbf{v}\|_H}{\|\mathbf{v}\|_H}. \tag{2.12}$$

A more general definition for the norm of a matrix is given in Definition 3.3.

The existence and uniqueness of the solution of the weak problem (2.5) comes from the theory of Brezzi–Fortin [7, 8]. For proofs that the bilinear forms and linear functionals in (2.5) satisfy the necessary and sufficient conditions to apply the Brezzi–Fortin theory; see [12] for the continuous finite element case and [28] for discontinuous Galerkin methods.

We remark that if the standard continuous Galerkin (CG) method is used to solve for the flow in both the Stokes and Darcy regions, then the matrices A_{Ω_1}, A_{Ω_2}

are both symmetric and positive definite. However, due to the interface block $A_{\Gamma_{12}}$, the $(1,1)$-block, A, of the saddle point matrix $\mathcal{A}$ is nonsymmetric. It is possible to maintain symmetry of the system matrix by scaling both the second and third rows of the block matrix $\mathcal{A}$ in (2.9). This gives a symmetric but indefinite matrix A, for which the coefficient matrix $\mathcal{A}$ could be solved by preconditioned MINRES [26]. Moreover, the symmetric preconditioners we introduce in the following section, including the constraint preconditioner, could be used. Though it is standard to use an s.p.d. preconditioner with MINRES, it is also possible to use a symmetric but indefinite constraint preconditioner. For complete details we refer the reader to the recent paper [18]. However, we do not consider symmetrizing the system since the block lower triangular preconditioners and one of the constraint preconditioners we consider are nonsymmetric. Furthermore, one could also model the flow in the Darcy region using a nonsymmetric discontinuous Galerkin (DG) method, as proposed in [11], in which case the matrix A_{Ω_2} is nonsymmetric, making $\mathcal{A}$ nonsymmetrizable.

3. Preconditioning. To determine the discrete Stokes velocity, Stokes pressure, and Darcy pressure we solve the large, sparse, and nonsymmetric saddle point matrix $\mathcal{A}$ with preconditioned GMRES [30]. We consider the following preconditioners:

$$\mathcal{P}_+ = \begin{bmatrix} A_{\Omega_2} & 0 & 0 \\ 0 & A_{\Omega_1} & 0 \\ 0 & 0 & M_p \end{bmatrix}, \qquad \mathcal{P}_{T_1}(\rho) = \begin{bmatrix} A_{\Omega_2} & 0 & 0 \\ 0 & A_{\Omega_1} & 0 \\ 0 & B & -\rho M_p \end{bmatrix},$$

$$\mathcal{P}_{T_2}(\rho) = \begin{bmatrix} A_{\Omega_2} & 0 & 0 \\ -A_{\Gamma_{12}} & A_{\Omega_1} & 0 \\ 0 & B & -\rho M_p \end{bmatrix}, \quad \mathcal{P}_C(\rho) = \begin{bmatrix} A_{\Omega_2} & A_{\Gamma_{12}}^T & 0 \\ -A_{\Gamma_{12}} & A_{\Omega_1} & 0 \\ 0 & B & -\rho M_p \end{bmatrix},$$

where M_p is the mass matrix coming from the Stokes pressure space. The matrix M_p is spectrally equivalent to the Schur complement of the Stokes operator [13, section 5.5.1].

These preconditioners were examined in [10] and are standard block diagonal and block triangular preconditioners. Moreover, utilizing the theory established in [24], Cai, Mu, and Xu [10] showed that the preconditioned operator $\mathcal{P}^{-1}\mathcal{A}$ with $\mathcal{P}$ of the above form has a spectrum that is bounded independently of the mesh width, or equivalently, of the order of the matrix, in the finite element discretization.

However, constraint preconditioners (see, e.g., [21, 27, 32]) were not addressed in [10]. We consider the following two constraint preconditioners, which we denote generically as $\mathcal{P}_{con}$:

$$\mathcal{P}_{con_D} = \begin{bmatrix} A_{\Omega_2} & 0 & 0 \\ 0 & A_{\Omega_1} & B^T \\ 0 & B & 0 \end{bmatrix}, \mathcal{P}_{con_T} = \begin{bmatrix} A_{\Omega_2} & 0 & 0 \\ -A_{\Gamma_{12}} & A_{\Omega_1} & B^T \\ 0 & B & 0 \end{bmatrix}.$$

The theory presented in [24] briefly mentions constraint preconditioners, and therefore we extend this theory by first proving norm-equivalence of $\mathcal{P}_{con}$ to the operator $\mathcal{A}$ and then proving the stronger result that $\mathcal{P}_{con}$ is f.o.v. equivalent to the operator $\mathcal{A}$.

Recall the saddle point system (2.10). Here, we consider $A \in \mathbb{R}^{n_1 \times n_1}$, $C \in \mathbb{R}^{n_2 \times n_1}$. It is assumed that the matrix $\mathcal{A} \in \mathbb{R}^{n \times n}$ satisfies the following stability conditions:

$$\max_{\mathbf{w} \in \mathbb{R}^n \setminus \{0\}} \max_{\mathbf{v} \in \mathbb{R}^n \setminus \{0\}} \frac{\mathbf{w}^T \mathcal{A} \mathbf{v}}{\|\mathbf{w}\|_H \|\mathbf{v}\|_H} \leq c_1, \tag{3.1a}$$

$$\min_{\mathbf{w} \in \mathbb{R}^n \setminus \{0\}} \max_{\mathbf{v} \in \mathbb{R}^n \setminus \{0\}} \frac{\mathbf{w}^T \mathcal{A} \mathbf{v}}{\|\mathbf{w}\|_H \|\mathbf{v}\|_H} \geq c_2, \tag{3.1b}$$

where H is an appropriate symmetric and positive definite matrix such that c_1, c_2 are positive constants independent of $n = n_1 + n_2$. Note that these stability conditions depend on the matrix H for which the norm is defined.

We show next that the constraint preconditioner

$$\mathcal{P}_{con} = \begin{bmatrix} P & C^T \\ C & 0 \end{bmatrix} \tag{3.2}$$

is H-norm equivalent (and subsequently H-f.o.v. equivalent) to the operator $\mathcal{A}$, where

$$H = \begin{bmatrix} H_1 & 0 \\ 0 & H_2 \end{bmatrix} \tag{3.3}$$

and H_1, H_2 are s.p.d. matrices. We use this H for the theoretical results though in experiments we measure convergence in the 2-norm, as was done in [10, 24]. Justification of the use of the 2-norm to measure convergence of the residuals in the numerical experiments is given, for instance, in [24, Remark 4.1] and [13, Theorem 6.9].

In the context of the coupled Stokes–Darcy problem

$$H_1 = \begin{bmatrix} A_{\Omega_2} & 0 \\ 0 & A_{\Omega_1} \end{bmatrix}, \quad H_2 = M_p,$$

which correspond to the discrete norms in (2.11).

Recall the definitions of H-norm and H-field-of-values-equivalence.

DEFINITION 3.1. *Two nonsingular matrices $M, N \in \mathbb{R}^{n\times n}$ are H-norm-equivalent, $M \sim_H N$, if there exist α_0, β_0 independent of n such that the following holds for all $\mathbf{x} \in \mathbb{R}^n \backslash \{0\}$:*

$$\alpha_0 \leq \frac{\|M\mathbf{x}\|_H}{\|N\mathbf{x}\|_H} \leq \beta_0. \tag{3.4}$$

As a consequence, $M \sim_H N$ is equivalent to

$$\|MN^{-1}\|_H \leq \beta_0, \tag{3.5a}$$

$$\|NM^{-1}\|_H \leq \alpha_0^{-1}. \tag{3.5b}$$

It can be shown that H-norm-equivalence is an equivalence relation, so in particular, if $M \sim_H N$, then $N \sim_H M$, and, if $M \sim_H N$ and $N \sim_H L$, then $M \sim_H L$.

DEFINITION 3.2. *Two nonsingular matrices $M, N \in \mathbb{R}^{n\times n}$ are H-field-of-values-equivalent, $M \approx_H N$, if there exist positive constants α_0, β_0 independent of n such that the following holds for all $\mathbf{x} \in \mathbb{R}^n \backslash \{0\}$:*

$$\alpha_0 \leq \frac{\langle MN^{-1}\mathbf{x}, \mathbf{x}\rangle_H}{\langle \mathbf{x}, \mathbf{x}\rangle_H} \quad \textit{and} \quad \|MN^{-1}\|_H \leq \beta_0.$$

We remark that f.o.v.-equivalence becomes spectral equivalence if the matrices M and N are symmetric positive definite and $H = I$; see [14, 21].

DEFINITION 3.3. *Let $M \in \mathbb{R}^{m\times n}$ and $H_1 \in \mathbb{R}^{n\times n}$, $H_2 \in \mathbb{R}^{m\times m}$ be two s.p.d. matrices, and then*

$$\|M\|_{H_1,H_2} = \max_{\mathbf{v}\in\mathbb{R}^n\backslash\{0\}} \frac{\|M\mathbf{v}\|_{H_2}}{\|\mathbf{v}\|_{H_1}}.$$

When $H_1 = H_2 = H$ and $m = n$, we recover the standard induced matrix norm (cf. (2.12))

$$\|M\|_{H,H} = \|M\|_H. \tag{3.6}$$

Moreover, we have the following useful set of equalities:

$$\|H_2^{-1/2} M H_1^{-1/2}\|_2 = \|M\|_{H_1,H_2^{-1}} = \|MH_1^{-1}\|_{H_1^{-1},H_2^{-1}} = \|H_2^{-1}M\|_{H_1,H_2}. \tag{3.7}$$

Observe that when $H_1 = H_2 = H$ in (3.7), we obtain (cf. (3.6))

$$\|H^{-1/2} M H^{-1/2}\|_2 = \|MH^{-1}\|_{H^{-1}} = \|H^{-1}M\|_H. \tag{3.8}$$

Additionally, if H_3 is also s.p.d., then the following matrix norm inequality holds:

$$\|MN\|_{H_3,H_1} \le \|N\|_{H_3,H_2}\|M\|_{H_2,H_1}. \tag{3.9}$$

We state the following lemmas proved by Loghin and Wathen [24].

LEMMA 3.4. *Let* (3.1) *hold, then* $H \sim_{H^{-1}} \mathcal{A}$ *and* $H^{-1} \sim_H \mathcal{A}^{-1}$, *and in particular*

$$\|H^{-1}\mathcal{A}\|_H = \|\mathcal{A}H^{-1}\|_{H^{-1}} \le c_1, \tag{3.10a}$$

$$\|\mathcal{A}^{-1}H\|_H = \|H\mathcal{A}^{-1}\|_{H^{-1}} \le c_2^{-1}. \tag{3.10b}$$

LEMMA 3.5. *Let* (3.1) *hold and assume* $\mathcal{P} \sim_{H^{-1}} H$, *then*

$$\mathcal{P} \sim_{H^{-1}} \mathcal{A} \quad \textit{and} \quad \mathcal{P}^{-1} \sim_H \mathcal{A}^{-1}.$$

LEMMA 3.6. *Let* (3.1) *hold, then* $\|A\|_{H_1,H_1^{-1}} \le c_1$, $\|C\|_{H_1,H_2^{-1}} \le c_1$.

LEMMA 3.7. *Let* (3.1) *hold. If there exists* c_3 *independent of* n *such that*

$$\min_{\mathbf{w}\in\mathbb{R}^n\setminus\{0\}} \max_{\mathbf{v}\in\mathbb{R}^n\setminus\{0\}} \frac{\mathbf{w}^T A \mathbf{v}}{\|\mathbf{w}\|_{H_1}\|\mathbf{v}\|_{H_1}} \ge c_3,$$

then $S = CA^{-1}C^T$, *the negative Schur complement, satisfies* $S \sim_{H_2^{-1}} H_2$ *and* $H_2^{-1} \sim_{H_2} S^{-1}$. *Hence, there exists* c_4 *independent of* n *such that* $\|S^{-1}\|_{H_2^{-1},H_2} \le c_4$.

It is worth noting that if A is replaced by an approximation $\tilde{A}$, then the previous lemma still holds for the corresponding approximate Schur complement, $\tilde{S} = C\tilde{A}^{-1}C^T$.

LEMMA 3.8. $\|M\|_{H_1,H_2^{-1}} = \|M^T\|_{H_2,H_1^{-1}}$.

We now present a new theorem on the norm-equivalence of constraint preconditioners.

THEOREM 3.9. *Let* $\mathcal{P}_{con}$ *be defined as in* (3.2), *let* H *be as in* (3.3), *and let* (3.1) *and the hypotheses of Lemma* 3.7 *hold. If* $P \sim_{H_1^{-1}} H_1$, *then* $\mathcal{P}_{con} \sim_{H^{-1}} \mathcal{A}$ *and* $\mathcal{P}_{con}^{-1} \sim_H \mathcal{A}^{-1}$.

Proof. By Lemma 3.5 all we need to show is that $\mathcal{P}_{con} \sim_{H^{-1}} H$. To prove this equivalence we bound both $\|\mathcal{P}_{con}H^{-1}\|_{H^{-1}} = \|H^{-1/2}\mathcal{P}_{con}H^{-1/2}\|_2$ and $\|H\mathcal{P}_{con}^{-1}\|_{H^{-1}} = \|H^{1/2}\mathcal{P}_{con}^{-1}H^{1/2}\|_2$. By the assumption that $P \sim_{H_1^{-1}} H_1$ we know there exist positive α_1, β_1, such that $\|PH_1^{-1}\|_{H_1^{-1}} \le \beta_1$ and $\|H_1P^{-1}\|_{H_1^{-1}} \le \alpha_1^{-1}$. Now consider

$$H^{-1/2}\mathcal{P}_{con}H^{-1/2} = \begin{bmatrix} H_1^{-1/2}PH_1^{-1/2} & H_1^{-1/2}C^TH_2^{-1/2} \\ H_2^{-1/2}CH_1^{-1/2} & 0 \end{bmatrix}. \tag{3.11}$$

We can bound the 2-norm of the above matrix as follows:

$$\begin{aligned}\|H^{-1/2}\mathcal{P}_{con}H^{-1/2}\|_2 &\le \|H_1^{-1/2}PH_1^{-1/2}\|_2 + \|H_2^{-1/2}CH_1^{-1/2}\|_2 + \|H_1^{-1/2}C^TH_2^{-1/2}\|_2\\ &= \|PH_1^{-1}\|_{H_1^{-1}} + \|C\|_{H_1,H_2^{-1}} + \|C^T\|_{H_2,H_1^{-1}}\\ &\le \beta_1 + c_1 + c_1.\end{aligned}$$

The first inequality is a result of expressing the block matrix as a sum of three matrices. The equality in the second line is obtained using (3.7) and Lemma 3.8. Last, the final bound comes from (3.1) (cf. Lemma 3.5) and the fact that $\|PH_1^{-1}\|_{H_1^{-1}} \le \beta_1$.

The inverse of $\mathcal{P}_{con}$ is

$$\mathcal{P}_{con}^{-1} = \begin{bmatrix} P^{-1} + P^{-1}C^TS^{-1}CP^{-1} & -P^{-1}C^TS^{-1} \\ -S^{-1}CP^{-1} & S^{-1}\end{bmatrix},$$

and therefore

$$H^{1/2}\mathcal{P}_{con}^{-1}H^{1/2} = \begin{bmatrix} H_1^{1/2}(P^{-1} + P^{-1}C^TS^{-1}CP^{-1})H_1^{1/2} & -H_1^{1/2}(P^{-1}C^TS^{-1})H_2^{1/2} \\ -H_2^{1/2}(S^{-1}CP^{-1})H_1^{1/2} & H_2^{1/2}S^{-1}H_2^{1/2}\end{bmatrix}.$$

Hence, $\|H^{1/2}\mathcal{P}_{con}^{-1}H^{1/2}\|_2$ can be bounded by bounding from above the five terms

$$\begin{aligned}(I) &= \|H_1^{1/2}P^{-1}H_1^{1/2}\|_2,\\ (II) &= \|H_1^{1/2}P^{-1}C^TS^{-1}CP^{-1}H_1^{1/2}\|_2,\\ (III) &= \|H_1^{1/2}P^{-1}C^TS^{-1}H_2^{1/2}\|_2,\\ (IV) &= \|H_2^{1/2}S^{-1}CP^{-1}H_1^{1/2}\|_2,\\ (V) &= \|H_2^{1/2}S^{-1}H_2^{1/2}\|_2.\end{aligned}$$

Recall that

$$(I) = \|H_1P^{-1}\|_{H_1^{-1}} \le \alpha_1^{-1},$$

and by Lemma 3.7

$$(V) = \|S^{-1}\|_{H_2^{-1},H_2} \le c_4.$$

Further note that

$$\begin{aligned}(II) &= \|H_1^{1/2}P^{-1}H_1^{1/2}H_1^{-1/2}C^TH_2^{-1/2}H_2^{1/2}S^{-1}H_2^{1/2}H_2^{-1/2}CH_1^{-1/2}H_1^{1/2}P^{-1}H_1^{1/2}\|_2\\ &\le \|H_1^{1/2}P^{-1}H_1^{1/2}\|_2\|H_1^{-1/2}C^TH_2^{-1/2}\|_2\|H_2^{1/2}S^{-1}H_2^{1/2}\|_2\\ &\quad \|H_2^{-1/2}CH_1^{-1/2}\|_2\|H_1^{1/2}P^{-1}H_1^{1/2}\|_2\\ &\le \alpha_1^{-1}c_1c_4c_1\alpha_1^{-1}.\end{aligned}$$

The terms (III) and (IV) are then bounded in a similar manner. ∎

With the aid of the previous theorem we show the following result on the H-f.o.v.-equivalence between $\mathcal{P}_{con}$ and $\mathcal{A}$.

THEOREM 3.10. *Let $\mathcal{A}, \mathcal{P}_{con}$ be defined as in* (2.10), (3.2), *respectively. Furthermore let* (3.1) *and the hypotheses of Lemma* 3.7 *hold. Let*

$$H = \begin{bmatrix}\rho H_1 & 0 \\ 0 & H_2\end{bmatrix}.$$

If $A \approx_{H_1^{-1}} P$, then there exists $\rho_0 > 0$ such that $\mathcal{A} \approx_{H^{-1}} \mathcal{P}_{con}$ for all $\rho \geq \rho_0$ provided $\|AP^{-1} - I\|_{H_1^{-1}} \leq \rho_0^{-1}$.

Proof. Since $A \approx_{H_1^{-1}} P$ there exist α_0, β_0 such that

$$\alpha_0 \leq \frac{\langle AP^{-1}x, x\rangle_{H_1^{-1}}}{\langle x, x\rangle_{H_1^{-1}}} \quad \text{and} \quad \|AP^{-1}\|_{H_1^{-1}} \leq \beta_0.$$

Moreover, f.o.v.-equivalence implies norm-equivalence so that we have $A \sim_{H_1^{-1}} P$ and due to (3.1), $A \sim_{H_1^{-1}} H_1$, we have $P \sim_{H_1^{-1}} H_1$. By Theorem 3.9, $\|\mathcal{A}\mathcal{P}_{con}^{-1}\|_{H^{-1}}$ is bounded from above. The only remaining piece is to show the existence of a lower bound

$$\alpha \mathbf{x}^T H^{-1} \mathbf{x} \leq \mathbf{x}^T H^{-1} \mathcal{A}\mathcal{P}_{con}^{-1} \mathbf{x}. \tag{3.12}$$

We have that

$$H^{-1}\mathcal{A}\mathcal{P}_{con}^{-1} = \begin{bmatrix} \rho H_1^{-1}(AP^{-1} - AP^{-1}C^T S^{-1} CP^{-1} + C^T S^{-1} CP^{-1}) & \rho H_1^{-1}(AP^{-1} - I)C^T S^{-1} \\ 0 & H_2^{-1} \end{bmatrix}.$$

Therefore, when $\mathbf{x} = \left[x_1^T, x_2^T\right]^T$, the product $\mathbf{x}^T H^{-1}\mathbf{x}$ is

$$\mathbf{x}^T H^{-1}\mathbf{x} = x_1^T H_1^{-1} x_1 + x_2^T H_2^{-1} x_2 = \|x_1\|^2_{H_1^{-1}} + \|x_2\|^2_{H_2^{-1}},$$

and $\mathbf{x}^T H^{-1}\mathcal{A}\mathcal{P}_{con}^{-1}\mathbf{x}$ is

$$\begin{aligned} \rho(x_1^T H_1^{-1} AP^{-1} x_1 \;+\; & x_1^T H_1^{-1}(I - AP^{-1})C^T S^{-1} CP^{-1} x_1) \\ +\; & \rho x_1^T H_1^{-1}(AP^{-1} - I)C^T S^{-1} x_2 \;+\; x_2^T H_2^{-1} x_2. \end{aligned} \tag{3.13}$$

Since $x_2^T H_2^{-1} x_2 = \|x_2\|^2_{H_2^{-1}}$, we establish the desired bound (3.12) by providing lower bounds for the other three terms, namely,

$$\begin{aligned} (I) &= x_1^T H_1^{-1} AP^{-1} x_1, \\ (II) &= x_1^T H_1^{-1}(I - AP^{-1})C^T S^{-1} CP^{-1} x_1, \\ (III) &= x_1^T H_1^{-1}(AP^{-1} - I)C^T S^{-1} x_2. \end{aligned}$$

For (I), by the f.o.v.-equivalence $A \approx_{H_1^{-1}} P$, there exists positive α_0 such that $x_1^T H_1^{-1} AP^{-1} x_1 \geq \alpha_0 \|x_1\|^2_{H_1^{-1}}$. In order to bound (II) from below, first consider the bound on the following absolute value, which is obtained using the Cauchy–Schwarz inequality

$$|\langle x_1, (I - AP^{-1})C^T S^{-1} CP^{-1} x_1\rangle_{H_1^{-1}}| \leq \|I - AP^{-1}\|_{H_1^{-1}} \|C^T S^{-1} CP^{-1}\|_{H_1^{-1}} \|x_1\|^2_{H_1^{-1}}.$$

From (3.7) we have

$$\begin{aligned} &\|C^T S^{-1} CP^{-1}\|_{H_1^{-1}} \\ &\quad = \|H_1^{-1/2} C^T S^{-1} CP^{-1} H_1^{1/2}\|_2 \\ &\quad \leq \|H_1^{-1/2} C^T H_2^{-1/2}\|_2 \|H_2^{1/2} S^{-1} H_2^{1/2}\|_2 \|H_2^{-1/2} C H_1^{-1/2}\|_2 \|H_1^{1/2} P^{-1} H_1^{1/2}\|_2 \\ &\quad \leq c_1^2 c_4 \alpha_1^{-1}, \end{aligned}$$

where c_1, c_2, and α_1 are as in Theorem 3.9.

Choosing $\|I - AP^{-1}\|_{H_1^{-1}} \leq \rho^{-1}$ and by negating the above absolute value we obtain

$$(II) \geq -\rho^{-1} c_1^2 c_4 \alpha_1^{-1} \|x_1\|_{H_1^{-1}}.$$

Last, for (III) we have that

$$\begin{aligned}
&|x_1^T H_1^{-1}(AP^{-1} - I)C^T S^{-1} x_2| \\
&\quad \leq \|(AP^{-1} - I)C^T S^{-1}\|_{H_2^{-1}, H_1^{-1}} \|x_1\|_{H_1^{-1}} \|x_2\|_{H_2^{-1}} \\
&\quad \leq \|C^T S^{-1}\|_{H_2^{-1}, H_1} \|AP^{-1} - I\|_{H_1^{-1}, H_1^{-1}} \|x_1\|_{H_1^{-1}} \|x_2\|_{H_2^{-1}} \\
&\quad \leq \|S^{-1}\|_{H_2^{-1}, H_2} \|C^T\|_{H_2, H_1^{-1}} \|AP^{-1} - I\|_{H_1^{-1}} \|x_1\|_{H_1^{-1}} \|x_2\|_{H_2^{-1}} \\
&\quad \leq c_1 c_4 \|AP^{-1} - I\|_{H_1^{-1}}.
\end{aligned}$$

Since $\|AP^{-1} - I\|_{H_1^{-1}} \leq \rho^{-1}$, we again negate the above absolute value to obtain a lower bound of the form

$$(III) \geq -\rho^{-1} c_1 c_4.$$

Combining these bounds and distributing ρ in (3.13), we obtain a lower bound of the form

$$(\rho a_1 - a_2)\|x_1\|_{H_1^{-1}}^2 - a_3 \|x_1\|_{H_1^{-1}} \|x_2\|_{H_2^{-1}} + \|x_2\|_{H_2^{-1}}^2, \tag{3.14}$$

where $a_1 = \alpha_0$, $a_2 = c_1^2 c_4 \alpha_1^{-1}$ and $a_3 = c_1 c_4$. By selecting $\rho := \rho_0 = (1 + a_3^2 + 2a_2)/2a_1$, (3.14) simplifies to

$$\begin{aligned}
&\frac{1 + a_3^2}{2} \|x_1\|_{H_1^{-1}}^2 - a_3 \|x_1\|_{H_1^{-1}} \|x_2\|_{H_2^{-1}} + \|x_2\|_{H_2^{-1}}^2 \\
&\quad = \frac{1}{2}\left(\|x_1\|_{H_1^{-1}}^2 + \|x_2\|_{H_2^{-1}}^2\right) + \frac{a_3^2}{2}\|x_1\|_{H_1^{-1}}^2 - a_3 \|x_1\|_{H_1^{-1}} \|x_2\|_{H_2^{-1}} + \frac{1}{2}\|x_2\|_{H_2^{-1}}^2 \\
&\quad = \frac{1}{2}\left(\|x_1\|_{H_1^{-1}}^2 + \|x_2\|_{H_2^{-1}}^2\right) + \frac{1}{2}\left(a_3 \|x_1\|_{H_1^{-1}} - \|x_2\|_{H_2^{-1}}\right)^2 \\
&\quad \geq \frac{1}{2}\left(\|x_1\|_{H_1^{-1}}^2 + \|x_2\|_{H_2^{-1}}^2\right).
\end{aligned}$$

This shows the existence, for $\rho_0 > 0$ defined as above, of the desired lower bound (3.12) of the form $\alpha \|\mathbf{x}\|_{H^{-1}}^2$ with $\alpha = 1/2$. Therefore, for any $\rho \geq \rho_0$, the above result holds. ∎

4. Inexact preconditioning. The theory of the previous section establishes f.o.v. bounds for the constraint preconditioned Stokes–Darcy system that are independent of the mesh-width when direct methods are used for the block solves. However, obtaining sufficiently resolved numerical solutions requires using small mesh widths, which translates into solving correspondingly larger linear systems. For these large-scale computations, particularly in three-dimensions, using direct methods for the block solves becomes prohibitively expensive. For practical computations, exact solves are replaced with fast, inexact methods that ideally maintain mesh-independent GMRES convergence. To ensure that the proven mesh-independent spectral bounds of the previous section hold, the exact block solves representing the underlying Darcy

and Stokes operators are replaced with spectrally equivalent multigrid operators. Recall that two s.p.d. matrices M and N are spectrally equivalent if there exist positive constants α, β independent of the mesh parameters such that for all $\mathbf{x} \neq 0$

$$\alpha < \frac{\langle M\mathbf{x}, \mathbf{x}\rangle}{\langle N\mathbf{x}, \mathbf{x}\rangle} < \beta. \tag{4.1}$$

The notion of spectral equivalence is important in establishing the mesh-independent convergence of multigrid methods for self-adjoint problems; cf. [13, 38]. As a consequence of this theory, the exact (direct) methods for the block solves in the preconditioners can be replaced by spectrally equivalent multigrid methods and still maintain the mesh-independent spectral properties. Here, we consider algebraic multigrid (AMG) methods; see, e.g., [6, 15, 29].

Specifically, we replace the inverse of P in the constraint preconditioner with the approximation

$$\tilde{P}^{-1} = \begin{bmatrix} \tilde{A}_{\Omega_2}^{-1} & 0 \\ 0 & \tilde{A}_{\Omega_1}^{-1} \end{bmatrix}, \tag{4.2}$$

where $\tilde{A}_{\Omega_2}^{-1}, \tilde{A}_{\Omega_1}^{-1}$ are AMG methods. Recall that for the case of continuous finite element basis functions, the matrices A_{Ω_1} and A_{Ω_2} are s.p.d.

Note that if $\tilde{A}_{\Omega_i}$ is spectrally equivalent to A_{Ω_i} for each i, then $\tilde{P}$ is spectrally equivalent to P. Then, by the change of variables $\mathbf{x} = \tilde{P}^{-1}\mathbf{y}$, (4.1) becomes a bound for all $\mathbf{y} \neq 0$

$$\alpha < \frac{\langle P\tilde{P}^{-1}\mathbf{y}, \tilde{P}^{-1}\mathbf{y}\rangle}{\langle \mathbf{y}, \tilde{P}^{-1}\mathbf{y}\rangle} < \beta. \tag{4.3}$$

In the following theorem we prove that the previous norm-equivalence still holds between $\mathcal{A}$ and a constraint preconditioner of the form

$$\tilde{\mathcal{P}}_{con} = \begin{bmatrix} \tilde{P} & C^T \\ C & 0 \end{bmatrix}, \tag{4.4}$$

where $\tilde{P}$ corresponds to the preconditioner defined in (4.2). This is the inexact analogue of Theorem 3.9.

THEOREM 4.1. *Let $\mathcal{A}$, $\tilde{\mathcal{P}}_{con}$ be defined as in* (2.10), (4.4), *respectively. Additionally, let* (3.1) *hold and the hypotheses of Lemma* 3.7 *hold but with A replaced by $\tilde{P}$. Let H be defined as in Theorem* 3.9. *If $\tilde{P}$ is spectrally equivalent to P, then the results of Theorem* 3.9 *remain true with $P = \tilde{P}$.*

Proof. Similar to the proof of Theorem 3.9, we establish H^{-1}-norm-equivalence of $\mathcal{A}$ to $\tilde{\mathcal{P}}_{con}$ by showing that $A \sim_{H_1^{-1}} \tilde{P}$. Recall that $A \sim_{H_1^{-1}} P$. We need only show that $P \sim_{H_1^{-1}} \tilde{P}$ as the desired norm-equivalence follows by transitivity. Thus, we provide upper and lower bounds on the term $\|P\tilde{P}^{-1}\|_{H_1^{-1}}$ (cf. Definition 3.1).

Using the spectral equivalence of $\tilde{P}$ with P, we show there exist mesh-independent upper and lower bounds on $\|P\tilde{P}^{-1}\|_{H_1^{-1}}$. By (4.3), we have

$$\alpha < \frac{\langle P\tilde{P}^{-1}\mathbf{x}, \tilde{P}^{-1}\mathbf{x}\rangle}{\langle \mathbf{x}, P^{-1}\mathbf{x}\rangle} \frac{\langle \mathbf{x}, P^{-1}\mathbf{x}\rangle}{\langle \mathbf{x}, \tilde{P}^{-1}\mathbf{x}\rangle} = \frac{\langle P\tilde{P}^{-1}\mathbf{x}, P\tilde{P}^{-1}\mathbf{x}\rangle_{H_1^{-1}}}{\langle \mathbf{x}, \mathbf{x}\rangle_{H_1^{-1}}} \frac{\langle \mathbf{x}, P^{-1}\mathbf{x}\rangle}{\langle \mathbf{x}, \tilde{P}^{-1}\mathbf{x}\rangle} < \beta.$$

Note that

$$\sup_{\mathbf{x}\neq 0} \frac{\langle P\tilde{P}^{-1}\mathbf{x}, P\tilde{P}^{-1}\mathbf{x}\rangle_{H_1^{-1}}}{\langle \mathbf{x}, \mathbf{x}\rangle_{H_1^{-1}}} = \|P\tilde{P}^{-1}\|_{H_1^{-1}}.$$

Spectral equivalence of two matrices, also implies spectral equivalence of their inverses, and thus there are mesh-independent bounds for the term

$$\frac{\langle \mathbf{x}, P^{-1}\mathbf{x}\rangle}{\langle \mathbf{x}, \tilde{P}^{-1}\mathbf{x}\rangle}.$$

As a result, $\|P\tilde{P}^{-1}\|_{H_1^{-1}}$ is bounded both above and below independently of the mesh width. Hence, $A \sim_{H_1^{-1}} \tilde{P}$. ∎

In order to apply the constraint preconditioner inexactly and in a manner consistent with the above theorem, we utilize the following block factorization with $S = -BA_{\Omega_1}^{-1}B^T$:

$$\begin{aligned}\mathcal{P}_{con_D}^{-1} &= \left(\begin{bmatrix} I & 0 & 0 \\ 0 & I & 0 \\ 0 & BA_{\Omega_1}^{-1} & I \end{bmatrix}\begin{bmatrix} A_{\Omega_2} & 0 & 0 \\ 0 & A_{\Omega_1} & 0 \\ 0 & 0 & S \end{bmatrix}\begin{bmatrix} I & 0 & 0 \\ 0 & I & A_{\Omega_1}^{-1}B^T \\ 0 & 0 & I \end{bmatrix}\right)^{-1} \\ &= \begin{bmatrix} I & 0 & 0 \\ 0 & I & -A_{\Omega_1}^{-1}B^T \\ 0 & 0 & I \end{bmatrix}\begin{bmatrix} A_{\Omega_2}^{-1} & 0 & 0 \\ 0 & A_{\Omega_1}^{-1} & 0 \\ 0 & 0 & S^{-1} \end{bmatrix}\begin{bmatrix} I & 0 & 0 \\ 0 & I & 0 \\ 0 & -BA_{\Omega_1}^{-1} & I \end{bmatrix}.\end{aligned}$$

The inexact constraint preconditioner then consists of replacing $A_{\Omega_i}^{-1}$ with an appropriate multigrid solver, which we denote by $\tilde{A}_{\Omega_i}^{-1}$ and the inverse Schur complement S^{-1} with the negative of the spectrally equivalent inverse pressure mass matrix M_p^{-1} [39]. One can either invert this matrix or invert its diagonal to maintain the spectral equivalence. In the numerical experiments, we use the latter approach since a diagonal matrix is trivial to invert.

The action of the above inexact constraint preconditioner on a vector $\mathbf{x} = [x, y, z]^T$ is

$$\begin{aligned}\mathcal{P}_{con_D}^{-1}\mathbf{x} &= \begin{bmatrix} I & 0 & 0 \\ 0 & I & -\tilde{A}_{\Omega_1}^{-1}B^T \\ 0 & 0 & I \end{bmatrix}\begin{bmatrix} \tilde{A}_{\Omega_2}^{-1} & 0 & 0 \\ 0 & \tilde{A}_{\Omega_1}^{-1} & 0 \\ 0 & 0 & M_p^{-1} \end{bmatrix}\begin{bmatrix} I & 0 & 0 \\ 0 & I & 0 \\ 0 & -B\tilde{A}_{\Omega_1}^{-1} & I \end{bmatrix}\begin{bmatrix} x \\ y \\ z \end{bmatrix} \\ &= \begin{bmatrix} \tilde{A}_{\Omega_2}^{-1}x \\ \tilde{A}_{\Omega_1}^{-1}y - \tilde{A}_{\Omega_1}^{-1}B^T M_p^{-1}(z - B\tilde{A}_{\Omega_1}^{-1}y) \\ M_p^{-1}(z - B\tilde{A}_{\Omega_1}^{-1}y) \end{bmatrix}.\end{aligned}$$

An application of the inexact constraint preconditioner amounts to one solve with $\tilde{A}_{\Omega_2}$, two solves with $\tilde{A}_{\Omega_1}$, one solve with M_p, and two additional matrix multiplications (one with B and one with B^T).

In the following section, we present numerical results where we compare the just described inexact implementation of the constraint preconditioner against the inexact implementations of the block diagonal preconditioner $\mathcal{P}_+$ and block lower triangular preconditioner $\mathcal{P}_{T_1}(\rho)$. The reason for using $\mathcal{P}_+$ and $\mathcal{P}_{T_1}$ is that they are the two most economical block diagonal and block lower triangular preconditioners to apply. Moreover, the performance of $\mathcal{P}_-$ and $\mathcal{P}_{T_2}$ does not differ significantly from $\mathcal{P}_+$ and $\mathcal{P}_{T_1}$. The comparison of these inexact preconditioners is done for two 3-D flow problems, and the results are presented in sections 5.2 and 5.3.

The inexact implementation of the block diagonal preconditioner consists of replacing each of the block solves with $\tilde{A}_{\Omega_2}$ and $\tilde{A}_{\Omega_1}$. The inexact implementation of $\mathcal{P}_{T_1}$ makes use of the following factorization:

$$\begin{aligned}\mathcal{P}_{T_1}^{-1}(\rho) &= \left(\begin{bmatrix} I & 0 & 0 \\ 0 & I & 0 \\ 0 & BA_{\Omega_1}^{-1} & I \end{bmatrix} \begin{bmatrix} A_{\Omega_2} & 0 & 0 \\ 0 & A_{\Omega_1} & 0 \\ 0 & 0 & -\rho M_p \end{bmatrix}\right)^{-1} \\ &= \begin{bmatrix} A_{\Omega_2}^{-1} & 0 & 0 \\ 0 & A_{\Omega_1}^{-1} & 0 \\ 0 & 0 & -\rho^{-1} M_p^{-1} \end{bmatrix} \begin{bmatrix} I & 0 & 0 \\ 0 & I & 0 \\ 0 & -BA_{\Omega_1}^{-1} & I \end{bmatrix}.\end{aligned}$$

Similar to the constraint preconditioner, the block operators $A_{\Omega_i}^{-1}$ are again replaced by the multigrid operators $\tilde{A}_{\Omega_i}^{-1}$.

The inexact version of the lower triangular preconditioner applied to a vector $\mathbf{x} = [x, y, z]^T$ is

$$\mathcal{P}_{T_1}^{-1}(\rho)\mathbf{x} = \begin{bmatrix} \tilde{A}_{\Omega_2}^{-1} x \\ \tilde{A}_{\Omega_1}^{-1} y \\ -\rho^{-1} M_p^{-1}(z - B\tilde{A}_{\Omega_1}^{-1} y) \end{bmatrix}. \tag{4.5}$$

The inexact implementation of $\mathcal{P}_{T_1}^{-1}$ involves one less solve with the operator $\tilde{A}_{\Omega_1}$ and one less matrix multiplication. We only consider the block lower triangular preconditioner $\mathcal{P}_{T_1}^{-1}$ for the inexact numerical experiments since it is the cheapest to apply in terms of computing time. In terms of operations, the most economical preconditioner to apply is the block diagonal preconditioner, followed by the lower triangular, and then constraint.

Last, we remark that in the 3-D experiments where the inexact preconditioners are used, the operators $\tilde{A}_{\Omega_1}$ and $\tilde{A}_{\Omega_2}$ correspond to calls to the smoothed aggregation AMG preconditioner in the ML package inside of Trilinos [16]. The smoothed aggregation multigrid algorithm was introduced in [35, 36]. The convergence analysis for this method is presented in [37], where it is shown that the bound on the condition number only increases as a polynomial in the number of levels.

In our numerical experiments, we set the AMG parameters as follows. The smoother is two Chebyshev iterations where the interval $[-1, 1]$ is mapped to an ellipse that contains computed estimates of the maximum and minimum eigenvalues. The aggregation threshold is set to 0.02. We also investigate the effect the number of AMG V-cycles has on the convergence of the solver. We consider values of $\{1, 4, 8\}$ for the number of cycles. As the number of cycles increase, the inner solves become more accurate and the number of outer iterations grows less with each mesh refinement. With more cycles, the accuracy of the inner solves approaches the exact field-of-values case where we do have mesh-independent convergence properties.

5. Numerical results. In this section, we present numerical results for both 2-D and 3-D problems for the coupled Stokes–Darcy system. For the 2-D problem the preconditioners are applied exactly, that is, they are calls to sparse direct solvers. The 3-D problems are implemented using the finite element library `deal.II` [3]. The first 3-D problem depicts a coupled flow in a rectangular channel where the free flow (Stokes) region is more elongated than the Darcy flow region. This type of setup was considered in [20]. The second problem is flow in a cubic domain where the Darcy domain contains a smaller impermeable cube in the center (see Figure 8). The 3-D numerical experiments are computed in serial using the high performance computing

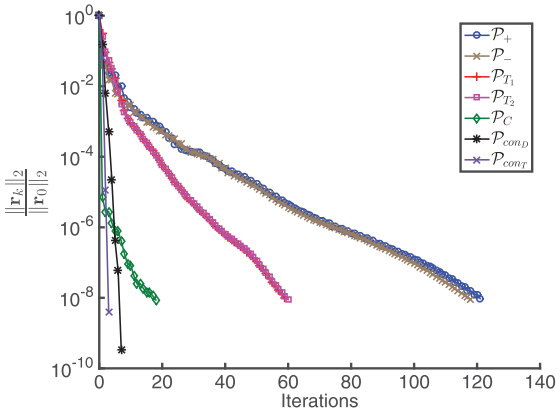

FIG. 2. *Residual convergence curves of the preconditioned GMRES algorithm on Problem* (5.1) *with* $\kappa = 1$ *and* $\nu = 1$. *The order of the system matrix is* $n = 524545$.

cluster, Owl's Nest, at Temple University on a subsection of the cluster with eight 2x Intel Xeon X5677 3.5 GHz processors with 96GB of memory per node [1].

5.1. 2-D flow with a smooth solution. We first consider a 2-D problem with $\Omega_1 = [0,1]^2$ and $\Omega_2 = [0,1] \times [1,2]$. We impose Neumann and Dirichlet boundary conditions on the lateral and horizontal parts of Γ_2, respectively; see Figure 1. The boundary conditions and data functions of the coupled Stokes–Darcy system are chosen so that the exact solution satisfies

$$\begin{cases} \mathbf{u}_1(x,y) = \left[y^2 - 2y + 1 + \nu(2x-1),\ x^2 - x - (y-1)2\nu\right]^T, \\ p_1(x,y) = 2\nu(x+y-1) + \dfrac{1}{3\kappa} - 4\nu^2, \\ p_2(x,y) = \dfrac{1}{\kappa}\left(x(1-x)(y-1) + \dfrac{y^3}{3} - y^2 + y\right) + 2\nu x. \end{cases} \tag{5.1}$$

For this problem, $\mathbf{K} = \kappa\mathbf{I}$, and we set $\kappa = \nu = 1$ and $G = 1.0$. The solution is computed on a mesh with triangular elements. For the Stokes velocity and pressure basis functions we use MINI finite elements. For the Darcy pressure basis functions we consider piecewise linear elements. We solve the discrete linear system using preconditioned GMRES. The stopping criterion for the algorithm is when $\|\mathbf{r}_k\|_2/\|\mathbf{r}_0\|_2 < 10^{-8}$. We remark that for finer meshes a more stringent tolerance may be more appropriate. The GMRES residual convergence curves for the considered preconditioners are displayed in Figure 2. The figure corresponds to a mesh width of $h = 2^{-8}$ for which the system matrix order is $n = 524545$. Observe that it takes under ten iterations for the preconditioned GMRES algorithm to converge using $\mathcal{P}_{con_D}$ and $\mathcal{P}_{con_T}$. In addition, the performance of the two block diagonal preconditioners, $\mathcal{P}_+, \mathcal{P}_-$, and the two block lower triangular preconditioners, $\mathcal{P}_{T_1}, \mathcal{P}_{T_2}$, are nearly identical.

We mention that we carried out additional experiments where we considered the effect on the number of iterations (and CPU times) for each preconditioner when both the viscosity and permeability parameters (ν and κ, respectively) are varied. The number of iterations and time it takes to converge increases for each preconditioner when the values of ν and κ are decreased. Thus, decreasing these values corresponds to making the coupled problem more difficult. Despite these problems being more challenging for each of the preconditioners, the results of our experiments illustrate

TABLE 1
Number of iterations and CPU times for convergence of Problem (5.1) *with* $\kappa = 1$, $\nu = 1$.

h	DOF	$\mathcal{P}_+$	$\mathcal{P}_{T_2}(0.6)$	$\mathcal{P}_C(0.6)$	$\mathcal{P}_{con_D}$	$\mathcal{P}_{con_T}$
2^{-3}	521	69 (0.11)	43 (0.04)	37 (0.03)	7 (0.01)	4 (0.01)
2^{-4}	2065	79 (0.24)	51 (0.12)	39 (0.09)	7 (0.02)	3 (0.02)
2^{-5}	8225	83 (0.95)	56 (0.60)	36 (0.37)	7 (0.14)	3 (0.10)
2^{-6}	32833	76 (4.40)	52 (3.12)	31 (1.89)	7 (0.82)	3 (0.63)
2^{-7}	131201	66 (19.0)	45 (13.6)	26 (8.11)	7 (4.33)	3 (3.89)
2^{-8}	524545	49 (82.0)	34 (55.9)	18 (29.9)	7 (23.5)	3 (22.5)

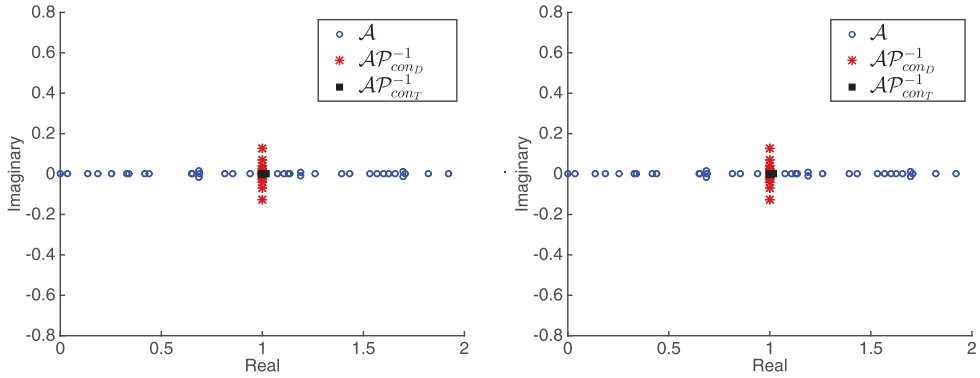

(a) Spectrum, $h = 2^{-3}$, $n = 521$ (b) Spectrum, $h = 2^{-4}$, $n = 2065$

FIG. 3. *Spectra of* $\Lambda(\mathcal{AP}^{-1}_{con_i})$ *for* $i = D, T$. *The circles, squares, and stars are the eigenvalues of* $\mathcal{A}$, $\mathcal{AP}^{-1}_{con_D}$, *and* $\mathcal{AP}^{-1}_{con_T}$, *respectively.*

the robustness of the constraint preconditioner over a range of values ν and κ; see [22] for complete details.

In order to further demonstrate the favorable properties of the two constraint preconditioners, we report in Table 1 both the iteration counts and CPU times as the mesh is uniformly refined. Observe that the constraint preconditioners give superior results both in terms of iteration count and CPU times.

This problem serves as a simple test case and shows the expected mesh-independent convergence properties for the constraint preconditioners. For some of the smaller sized problems, we computed the spectra of the constraint preconditioned operators to visually illustrate Theorem 3.9. For this specific problem, the computed spectra of $\Lambda(\mathcal{A})$, $\Lambda(\mathcal{AP}^{-1}_{con_D})$, and $\Lambda(\mathcal{AP}^{-1}_{con_T})$ are displayed in Figure 3 (as circles, stars, and squares, respectively). The matrices correspond to mesh widths of $h = 2^{-3}, 2^{-4}$ (system orders $n = 521$ and 2065, respectively). Observe that the spectra are bounded, which is a direct consequence of Theorem 3.9.

5.2. 3-D rectangular channel flow. In this set of experiments, we consider coupled Stokes–Darcy flow in a rectangular prism with $\Omega_1 = [0, 0.05]^2 \times [0.1, 0.25]$ and $\Omega_2 = [0, 0.05]^2 \times [0, 0.1]$. The interface Γ_{12} is the plane $z = 0.10$; see Figure 4. Along $z = 0.25$ on the Stokes boundary $\Gamma_{1,in}$, we prescribe

$$\mathbf{u}_1 = (0, 0, -0.1)^T.$$

On the rest of the Stokes boundary we prescribe a no-slip condition, i.e.,

$$\mathbf{u}_1 = (0, 0, 0)^T \text{ on } \Gamma_{1,0}.$$

On the boundary of the porous medium we prescribe homogeneous Dirichlet boundary

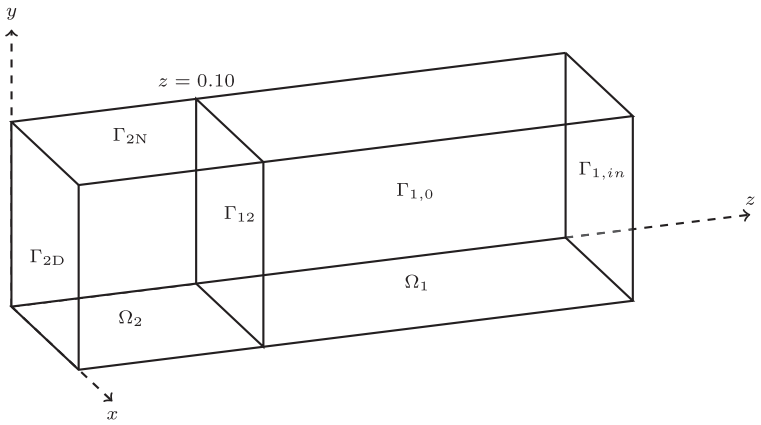

FIG. 4. *Computational domain for rectangular channel flow.*

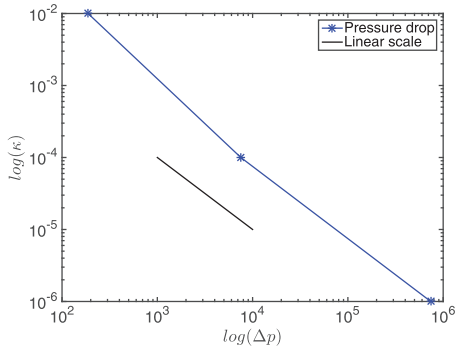

FIG. 5. *Log-log plot of the pressure drop in the Darcy domain as the permeability κ is decreased for the channel flow problem. The pressure values were taken from computations on the finest mesh with $h = 0.00025$ using $\mathcal{P}_{con_D}$ with eight AMG cycles.*

conditions on the plane $z = 0$ ($\Gamma_{2\mathrm{D}}$) and homogeneous Neumann boundary conditions on the rest of the boundary, corresponding to zero flux and pressure on the respective boundaries, i.e., $g_{\mathrm{N}} = g_{\mathrm{D}} = 0$. The rest of the constants and data are defined as

$$\mathbf{f}_1 = (0, 0, 0)^T, \quad f_2 = 0, \text{ and } \nu = 1.0 \ .$$

In this problem, the hydraulic conductivity $\mathbf{K} = \kappa\mathbf{I}$ with $\kappa \in \{10^{-2}, 10^{-4}, 10^{-6}\}$. The reason for varying the permeability is to illustrate the robustness of the inexact constraint preconditioner in addition to demonstrating how the proposed solver is able to reproduce the expected linear drop in pressure as κ is decreased; see Figure 5. We solve the discrete Stokes–Darcy linear system using the inexact versions of the preconditioners described in section 4. The stopping criterion is $\|\mathbf{r}_k\|_2/\|\mathbf{r}_0\|_2 < 10^{-6}$. Since the inexact versions of these preconditioners are calls to a fixed number of AMG cycles at each iteration, we can still use GMRES as the solver.[1] The number of iterations and CPU times are given in Tables 2–4. Observe that as the permeability κ decreases, the number of iterations for each preconditioner increases. In terms of iterations, the constraint preconditioner is superior except for when $\kappa = 10^{-6}$ and

[1] That is, there is no need to use a flexible Krylov subspace method.

TABLE 2

Table of GMRES iterations and CPU time (seconds) for the rectangular channel flow problem with $\kappa = 10^{-2}$.

h	elements	DOF	$\mathcal{P}_+$	$\mathcal{P}_{T_1}$	$\mathcal{P}_{con_D}$
0.01	625	14370	154 (6.679)	58 (2.500)	47 (3.527)
0.005	5000	102535	227 (81.66)	83 (29.51)	69 (42.65)
0.00025	40000	773265	442 (1389)	139 (408.9)	117 (595.8)

(a) 1 AMG cycle

h	elements	DOF	$\mathcal{P}_+$	$\mathcal{P}_{T_1}$	$\mathcal{P}_{con_D}$
0.01	625	14370	93 (14.93)	40 (6.514)	32 (10.03)
0.005	5000	102535	130 (175.5)	59 (79.61)	45 (116.8)
0.00025	40000	773265	259 (2908)	86 (959.6)	65 (1382)

(b) 4 AMG cycles

h	elements	DOF	$\mathcal{P}_+$	$\mathcal{P}_{T_1}$	$\mathcal{P}_{con_D}$
0.01	625	14370	79 (25.16)	38 (12.22)	27 (17.07)
0.005	5000	102535	107 (284.3)	52 (139.2)	32 (169.6)
0.00025	40000	773265	192 (4215)	71 (1572)	42 (1823)

(c) 8 AMG cycles

TABLE 3

Table of GMRES iterations and CPU time (seconds) for the rectangular channel flow problem with $\kappa = 10^{-4}$.

h	elements	DOF	$\mathcal{P}_+$	$\mathcal{P}_{T_1}$	$\mathcal{P}_{con_D}$
0.01	625	14370	178 (7.756)	70 (3.013)	57 (4.260)
0.005	5000	102535	237 (85.59)	94 (33.44)	77 (47.67)
0.00025	40000	773265	443 (1394)	136 (399.7)	112 (570.3)

(a) 1 AMG cycle

h	elements	DOF	$\mathcal{P}_+$	$\mathcal{P}_{T_1}$	$\mathcal{P}_{con_D}$
0.01	625	14370	116 (18.55)	53 (8.478)	46 (14.19)
0.005	5000	102535	159 (212.2)	69 (92.69)	58 (149.8)
0.00025	40000	773265	275 (3041)	98 (1078)	74 (1563)

(b) 4 AMG cycles

h	elements	DOF	$\mathcal{P}_+$	$\mathcal{P}_{T_1}$	$\mathcal{P}_{con_D}$
0.01	625	14370	103 (32.39)	51 (16.12)	40 (24.92)
0.005	5000	102535	138 (363.1)	61 (160.1)	47 (242.4)
0.00025	40000	773265	215 (4630)	85 (1839)	57 (2410)

(c) 8 AMG cycles

TABLE 4

Table of GMRES iterations and CPU time (seconds) for the rectangular channel flow problem with $\kappa = 10^{-6}$.

h	elements	DOF	$\mathcal{P}_+$	$\mathcal{P}_{T_1}$	$\mathcal{P}_{con_D}$
0.01	625	14370	369 (16.97)	171 (7.517)	158 (11.86)
0.005	5000	102535	558 (218.0)	229 (83.56)	189 (117.7)
0.00025	40000	773265	895 (3152)	270 (821.8)	240 (1243)

(a) 1 AMG cycle

h	elements	DOF	$\mathcal{P}_+$	$\mathcal{P}_{T_1}$	$\mathcal{P}_{con_D}$
0.01	625	14370	285 (46.10)	155 (24.97)	145 (44.78)
0.005	5000	102535	433 (595.7)	193 (259.6)	169 (434.3)
0.00025	40000	773265	630 (7283)	226 (2547)	229 (4896)

(b) 4 AMG cycles

h	elements	DOF	$\mathcal{P}_+$	$\mathcal{P}_{T_1}$	$\mathcal{P}_{con_D}$
0.01	625	14370	265 (84.18)	152 (48.44)	135 (83.17)
0.005	5000	102535	398 (1057)	181 (479.5)	155 (799.2)
0.00025	40000	773265	522 (11441)	203 (4428)	211 (9020)

(c) 8 AMG cycles

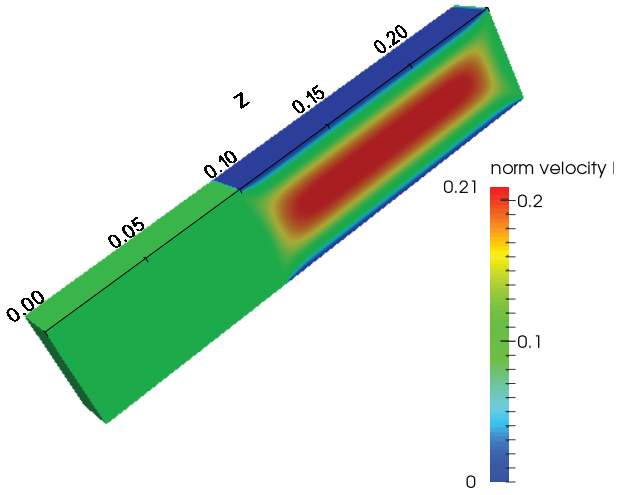

(a) Norm of velocity

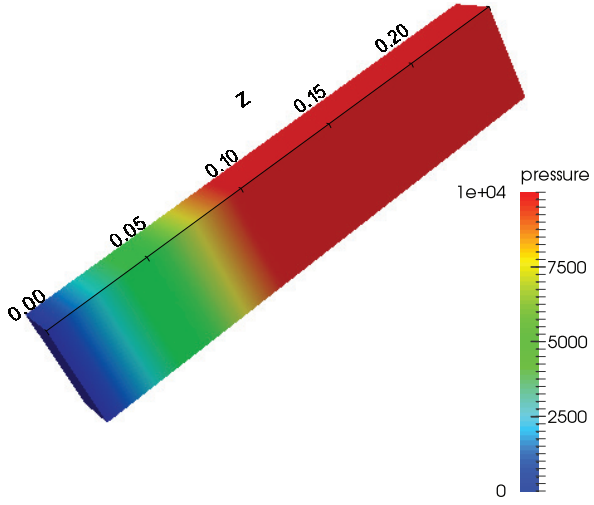

(b) Pressure

FIG. 6. *Slice of the numerical solution obtained using* $\mathcal{P}_{con_D}$ *with eight AMG cycles for rectangular channel flow along* $x = 0.025$ *with permeability* $\kappa = 10^{-6}$. *The problem size here is* $n = 773265$.

when more than one AMG cycle is used. The most economical preconditioner, giving the lowest CPU times, is the block lower triangular preconditioner. It is also clear that with more AMG cycles, corresponding to more accurate inner solves, the number of outer iterations grows less rapidly with the refinement of the mesh. These experiments were inspired by those in [20], where a similar computational setup was considered for a different problem, namely, the coupled Navier–Stokes–Darcy system.

We solve this problem on a mesh with hexahedral elements using the software package `deal.II` [3]. For the Stokes velocity and pressure basis functions we use the Taylor–Hood pair of biquadratic and bilinear finite elements, respectively. The Darcy pressure is approximated by continuous biquadratic elements.

Figure 6 is a plot of the numerical solution showing the coupled flow in a rectangular channel obtained on a uniform grid with mesh size $h = 0.00025$ from a coupled

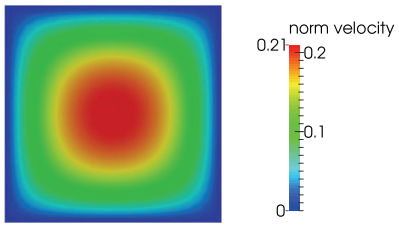

FIG. 7. *Cross section of the numerical solution using* $\mathcal{P}_{con_D}$ *with eight AMG cycles for channel flow along* $z = 0.02$ *with* $\kappa = 10^{-6}$. *The problem size here is* $n = 773265$.

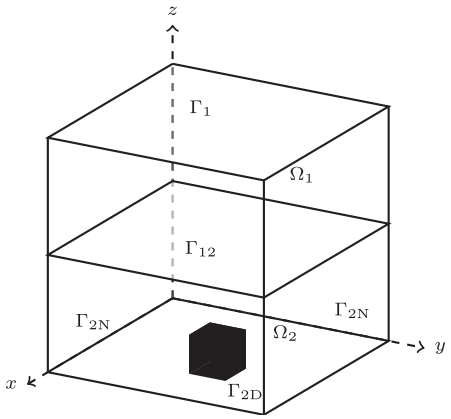

FIG. 8. *Computational domain with impermeable enclosure in* Ω_2.

system of order $n = 773265$. In Figure 6(a) we plot the norm of the velocity in both the Stokes and Darcy domains. As shown in Figure 7, we observe the expected parabolic increase in the norm of the velocity from zero at the no slip portion of the Stokes boundary to a maximum of 0.21 at the center of the domain. The low permeability in the porous medium results in build up of pressure in the free flow domain, and therefore we observe large values of pressure in Ω_1 and a gradual stratified drop in pressure to zero on the Dirichlet boundary of Ω_2, where homogeneous boundary conditions are imposed; see Figure 6(b).

5.3. Darcy domain with an impermeable enclosure. We consider a 3-D coupled flow problem, where the computational domain is a cube with $\Omega_1 = [0,2]^2 \times [1,2]$ and $\Omega_2 = [0,2]^2 \times [0,1]$. The porous medium contains an embedded impermeable cube $[0.75, 1.25]^2 \times [0.0, 0.50]$; see Figure 8. We denote the hydraulic conductivity of the porous medium and embedded impermeable enclosure by $\kappa_1 \mathbf{I}$ and $\kappa_2 \mathbf{I}$, respectively.

On the horizontal part of Γ_1 we prescribe

$$\mathbf{u}_1 = (0, 0, -1)^T \text{ on } z = 2.0$$

and the no-slip condition on the lateral sides of Γ_1. As in the previous example, we prescribe homogeneous Dirichlet boundary conditions on $z = 0$ (Γ_{2D}) and homogeneous Neumann boundary conditions on the rest of the boundary of the porous medium. The rest of the parameters and data functions are

$$\mathbf{f}_1 = (0, 0, 0)^T, \quad f_2 = 0, \quad \nu = 1.0, \quad \kappa_1 = 1, \text{ and } \kappa_2 = 10^{-10}.$$

TABLE 5

Table of GMRES iterations and CPU time (seconds) for the discontinuous permeability field with inexact preconditioners.

h	elements	DOF	$\mathcal{P}_+$	$\mathcal{P}_{T_1}$	$\mathcal{P}_{con_D}$
2^{-1}	64	1695	59 (0.312)	34 (0.188)	30 (0.276)
2^{-2}	512	10809	153 (4.638)	54 (1.637)	46 (2.386)
2^{-3}	4096	76653	250 (63.54)	64 (15.82)	56 (23.97)
2^{-4}	32768	576213	485 (1083)	116 (239.2)	99 (346.7)

(a) $\kappa_1 = 1$, $\kappa_2 = 10^{-10}$, 1 AMG cycles,

h	elements	DOF	$\mathcal{P}_+$	$\mathcal{P}_{T_1}$	$\mathcal{P}_{con_D}$
2^{-1}	64	1695	59 (0.927)	34 (0.548)	30 (0.907)
2^{-2}	512	10809	97 (10.70)	41 (4.526)	37 (7.920)
2^{-3}	4096	76653	144 (133.3)	52 (48.48)	43 (76.80)
2^{-4}	32768	576213	267 (2027)	69 (526.2)	55 (800.7)

(b) $\kappa_1 = 1$, $\kappa_2 = 10^{-10}$, 4 AMG cycles

h	elements	DOF	$\mathcal{P}_+$	$\mathcal{P}_{T_1}$	$\mathcal{P}_{con_D}$
2^{-1}	64	1695	59 (1.763)	34 (1.044)	30 (1.767)
2^{-2}	512	10809	86 (18.82)	40 (8.894)	36 (15.81)
2^{-3}	4096	76653	116 (213.1)	49 (90.91)	38 (137.2)
2^{-4}	32768	576213	200 (3022)	61 (931.8)	44 (1307)

(c) $\kappa_1 = 1$, $\kappa_2 = 10^{-10}$, 8 AMG cycles

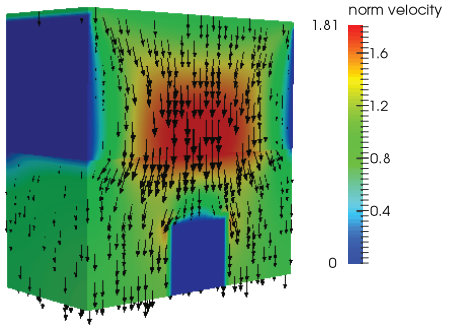

FIG. 9. *Slice of the numerical solution obtained using $\mathcal{P}_{con_D}$ with eight AMG cycles along $y = 0.5$ from the domain with an impermeable enclosure. The problem size is $n = 576213$.*

We again solve this discrete linear system using preconditioned GMRES with the inexact versions of the three preconditioners as described in section 4. The stopping criterion is $\|\mathbf{r}_k\|_2/\|\mathbf{r}_0\|_2 < 10^{-6}$. The number of GMRES iterations and CPU times are presented in Table 5.

Here, we observe similar results to the rectangular channel flow problem. There is moderate growth in the number of iterations as the mesh is uniformly refined, and with more AMG cycles the growth is much slower. The constraint preconditioner again gives superior iteration counts, but the most economical preconditioner in terms of CPU time is the block lower triangular preconditioner. We also remark that sparse direct solvers were competitive until the third level of refinement and ran out of memory for the matrix of order $n = 576213$.

In Figure 9 we plot the norm of the velocity along with normalized vectors showing the direction of the flow from a uniform mesh of size $h = 2^{-4}$ from a coupled system of order $n = 576213$. We observe the expected coupled flow pattern with the maximum

velocity observed on the central part of the Stokes domain flowing vertically downward and avoiding the impermeable cube. The presence of an impermeable enclosure with a low permeability ($\kappa_2 = 10^{-10}$) is clear.

6. Conclusions. We have examined the performance of standard block diagonal, block triangular, and constraint preconditioners for the sequential solution of the coupled Stokes–Darcy system. We have proved bounds on the spectrum and field of values of the constraint preconditioned operator that are independent of the underlying mesh discretization parameter. To illustrate our theoretical results, we considered the numerical solution of flow problems in both two and three dimensions. The experiments in two dimensions illustrate convergence of the GMRES algorithm in a number of iterations that is independent of the mesh-width when using exact versions of the constraint preconditioner. The experiments in three dimensions further demonstrate the favorable properties of the inexact constraint preconditioner. Though the mesh-independence convergence properties are no longer theoretically guaranteed, mesh-independent convergence can still be observed, provided the inexact solve is accurate enough. For the inexact case we can observe a slow growth in the number of iterations for all preconditioners, though the growth is slowest for the constraint preconditioner. This trend is also accentuated when more AMG cycles are performed. Our experiments also indicate that the constraint preconditioner is robust with respect to decreases in the permeability of the porous medium. In summary, constraint preconditioners offer another effective preconditioning technique for the solution of the linear system arising from the finite element discretization of the coupled Stokes–Darcy problem.

Acknowledgments. We thank Howard Elman and Panayot Vassilevski for useful discussions regarding spectrally equivalent multigrid methods. We also thank Valeria Simoncini, Andrew Wathen, and Walter Zuhlener for comments after talks the authors gave on preliminary results. Valeria Simoncini also made useful suggestions on an early version of this paper. Finally, we thank the reviewers and Chen Greif, the Associate Editor, for their careful reading and comments.

REFERENCES

[1] Owl's Nest High Performance Computing, Temple University, http://www.hpc.temple.edu/owlsnest/OwlsnestUserGuide.html.

[2] D. N. Arnold, F. Brezzi, and M. Fortin, *A stable finite element for the Stokes equations*, Calcolo, 21 (1984), pp. 337–344.

[3] W. Bangerth, T. Heister, L. Heltai, G. Kanschat, M. Kronbichler, M. Maier, B. Turcksin, and T. D. Young, *The* `deal.ii` *library, version* 8.1, preprint, http://arxiv.org/abs/1312.2266v4, 2013.

[4] G. S. Beavers and D. D. Joseph, *Boundary conditions at a naturally permeable wall*, J. Fluid Mech., 30 (1967), pp. 197–207.

[5] M. Benzi, G. H. Golub, and J. Liesen, *Numerical solution of saddle point problems*, Acta Numer., 14 (2005), pp. 1–137.

[6] A. Brandt, *Algebraic multigrid theory: The symmetric case*, Appl. Math. Comput., 19 (1986), pp. 23–56.

[7] F. Brezzi, *On the existence, uniqueness and approximation of saddle-point problems arising from Lagrangian multipliers*, ESAIM Math. Model. Numer. Anal., 8 (1974), pp. 129–151.

[8] F. Brezzi and M. Fortin, *Mixed and Hybrid Finite Element Methods*, Springer, New York, 1991.

[9] W. L. Briggs, V. E. Henson, and S. F. McCormick, *A Multigrid Tutorial*, 2nd ed., SIAM, Philadelphia, 2000.

[10] M. Cai, M. Mu, and J. Xu, *Preconditioning techniques for a mixed Stokes/Darcy model in porous media applications*, J. Comput. Appl. Math., 233 (2009), pp. 346–355.

[11] P. Chidyagwai and B. Rivière, *Numerical modelling of coupled surface and subsurface flow systems*, Adv. Water Res., 33 (2010), pp. 92–105.
[12] M. Discacciati and A. Quarteroni, *Navier–Stokes/Darcy coupling: Modeling, analysis, and numerical approximation*, Rev. Mat. Complut., 22 (2009), pp. 315–426.
[13] H. C. Elman, D. J. Silvester, and A. J. Wathen, *Finite Elements and Fast Iterative Solvers: With Applications in Incompressible Fluid Dynamics*, Oxford University Press, Oxford, 2005.
[14] V. Faber, T. A. Manteuffel, and S. V. Parter, *On the theory of equivalent operators and application to the numerical solution of uniformly elliptic partial differential equations*, Adv. Appl. Math., 11 (1990), pp. 109–163.
[15] R. D. Falgout and P. S. Vassilevski, *On generalizing the algebraic multigrid framework*, SIAM J. Numer. Anal., 42 (2004), pp. 1669–1693.
[16] M. W. Gee, C. M. Siefert, J. J. Hu, R. S. Tuminaro, and M. G. Sala, *ML* 5.0 *Smoothed Aggregation User's Guide*, Technical report SAND2006-2649, Sandia National Laboratories, 2006.
[17] V. Girault, D. Vassilev, and I. Yotov, *Mortar multiscale finite element methods for Stokes–Darcy flows*, Numer. Math., 127 (2013), pp. 1–73.
[18] N. Gould, D. Orban, and T. Rees, *Projected Krylov methods for saddle-point systems*, SIAM J. Matrix Anal. Appl., 35 (2014), pp. 1329–1343.
[19] W. Hackbusch, *Multi-Grid Methods and Applications*, Springer, New York, 1985.
[20] N. S. Hanspal, V. Nassehi, and A. Kulkarni, *Three-dimensional finite element modelling of coupled free/porous flows: Applications to industrial and environmental flows*, Int. J. Numer. Methods Fluids, 71 (2013), pp. 1382–1421.
[21] C. Keller, N. I. Gould, and A. J. Wathen, *Constraint preconditioning for indefinite linear systems*, SIAM J. Matrix Anal. Appl., 21 (2000), pp. 1300–1317.
[22] S. Ladenheim, *Constraint Preconditioning of Saddle Point Problems*, Ph.D. thesis, Temple University, Philadelphia, 2015.
[23] W. J. Layton, F. Schieweck, and I. Yotov, *Coupling fluid flow with porous media flow*, SIAM J. Numer. Anal., 40 (2002), pp. 2195–2218.
[24] D. Loghin and A. J. Wathen, *Analysis of preconditioners for saddle-point problems*, SIAM J. Sci. Comput., 25 (2004), pp. 2029–2049.
[25] A. Márquez, S. Meddahi, and F.-J. Sayas, *A decoupled preconditioning technique for a mixed Stokes–Darcy model*, J. Sci. Comput., 57 (2013), pp. 174–192.
[26] C. C. Paige and M. A. Saunders, *Solution of sparse indefinite systems of linear equations*, SIAM J. Numer. Anal., 12 (1975), pp. 617–629.
[27] I. Perugia and V. Simoncini, *Block-diagonal and indefinite symmetric preconditioners for mixed finite element formulations*, Numer. Linear Algebra Appl., 7 (2000), pp. 585–616.
[28] B. Rivière, *Analysis of a discontinuous finite element method for the coupled Stokes and Darcy problems*, J. Sci. Comput., 22 (2005), pp. 479–500.
[29] J. W. Ruge and K. Stüben, *Algebraic multigrid*, in Multigrid Methods, S. F. McCormick, ed., Front. Appl. Math. 3, SIAM, Philadelphia, 1987, pp. 73–130.
[30] Y. Saad and M. H. Schultz, *GMRES: A generalized minimal residual algorithm for solving nonsymmetric linear systems*, SIAM J. Sci. Stat. Comput., 7 (1986), pp. 856–869.
[31] P. G. Saffman, *On the boundary condition at the surface of a porous medium*, Stud. Appl. Math., 50 (1971), pp. 93–101.
[32] D. Sesana and V. Simoncini, *Spectral analysis of inexact constraint preconditioning for symmetric saddle point matrices*, Linear Algebra Appl., 438 (2013), pp. 2683–2700.
[33] V. Simoncini and D. B. Szyld, *Recent computational developments in Krylov subspace methods for linear systems*, Numer. Linear Algebra Appl., 14 (2007), pp. 1–59.
[34] C. Taylor and P. Hood, *A numerical solution of the Navier–Stokes equations using the finite element technique*, Comput. & Fluids, 1 (1973), pp. 73–100.
[35] P. Vaněk, *Acceleration of convergence of a two-level algorithm by smoothing transfer operators*, Appl. Math., 37 (1992), pp. 265–274.
[36] P. Vaněk, *Fast multigrid solver*, Appl. Math., 40 (1995), pp. 1–20.
[37] P. Vaněk, M. Brezina, and J. Mandel, *Convergence of algebraic multigrid based on smoothed aggregation*, Numer. Math., 88 (2001), pp. 559–579.
[38] P. S. Vassilevski, *Multilevel Block Factorization Preconditioners*, Springer, New York, 2008.
[39] A. J. Wathen, *Realistic eigenvalue bounds for the Galerkin mass matrix*, IMA J. Numer. Anal., 7 (1987), pp. 449–457.